Atmospheric plasma-polymerization of hydrophobic and wear-resistant coatings on glass substrates

Rodolfo Múgica-Vidal [(a)], Fernando Alba-Elías [(a)], Elisa Sainz-García [(a)], Joaquín Ordieres-Meré [(b)]

(a) Department of Mechanical Engineering. University of La Rioja. c/ Luis de Ulloa 20, 26004 Logroño, La Rioja, Spain.

(b) PMQ Research Team. ETSII. Polytechnic University of Madrid. c/ José Gutiérrez Abascal 2, 28006 Madrid, Spain.

Accepted Version for publication in Surface and Coatings Technology

Link to publisher version (DOI): https://doi.org/10.1016/J.SURFCOAT.2014.10.067

Published source citation:
Múgica-Vidal, R., Alba-Elías, F., Sainz-García, E., & Ordieres-Meré, J. (2014). Atmospheric plasma-polymerization of hydrophobic and wear-resistant coatings on glass substrates. *Surface and Coatings Technology*, *259*(PC), 374-385. https://doi.org/10.1016/J.SURFCOAT.2014.10.067

Author names and affiliations:

Rodolfo Múgica-Vidal
Department of Mechanical Engineering
University of La Rioja
c/ Luis de Ulloa 20, 26004 - Logroño, La Rioja, Spain.
Tel.: +34 941299276; fax: +34 941299794.
E-mail address: rodolfo.mugica@alum.unirioja.es

Elisa Sainz-García
Department of Mechanical Engineering
University of La Rioja
c/ Luis de Ulloa 20, 26004 - Logroño, La Rioja, Spain.
Tel.: +34 941299276; fax: +34 941299794.
E-mail address: elisa.sainzg@unirioja.es

Joaquín Ordieres-Meré
PMQ Research Team. ETSII.
Polytechnic University of Madrid.
c/ José Gutiérrez Abascal 2, 28006 - Madrid, Spain.
Tel.: +34 913364684; fax: +34 913363145.
E-mail address: j.ordieres@upm.es

Corresponding author:

Fernando Alba-Elías
Department of Mechanical Engineering
University of La Rioja
c/ Luis de Ulloa, 20, 26004 - Logroño, La Rioja, Spain.
Tel.: +34 941299276; fax: +34 941299794.
E-mail address: fernando.alba@unirioja.es

Abstract

In order to find a coating that promotes both the wear resistance and the hydrophobicity of glass, a non-thermal atmospheric jet plasma-polymerization system with mixtures of two precursors at different proportions were used. (Heptadecafluoro-1,1,2,2-tetrahydrodecyl)trimethoxysilane (FLUSI) was used to promote the hydrophobicity, due to its fluorocarbon chain. Aminopropyltriethoxysilane (APTES) was used to enhance the wear resistance of the surface. The key aspect of the present work consists of determining the optimal mixture of precursors that produces a satisfactory coating in both characteristics; since coatings based on FLUSI have a low wear resistance and those based on APTES have a hydrophilic character. Scanning Electron Microscopy (SEM), Atomic Force Microscopy (AFM), Fourier Transform Infrared spectroscopy (FTIR), X-Ray Photoelectron Spectroscopy (XPS), lap-shear tests, Static Water Contact Angle (WCA), tribological tests, profilometry measurements and Energy Dispersive X-Ray spectroscopy (EDX) were used to analyze the coatings. It is believed that the upper limit of hydrophobicity that can be attained by modifying of the surface chemistry (WCA of ~120º) has been achieved. It was observed that the wear resistance depends on the thickness and the SiOSi content of the coatings. These appear to be directly related to the proportion of APTES in the mixture. The sample that was coated with 50% of APTES and 50% of FLUSI provided the best combination of hydrophobicity and wear resistance. It showed the highest WCA (123.2º ± 1.5) because it has a high fluorocarbon content and the highest CF_3 content. Its wear resistance is considerably better than that of the uncoated glass and is one of the highest exhibited by the hydrophobic samples.

Keywords: Wear resistance; Hydrophobic; APTES; FLUSI; Non-thermal atmospheric jet plasma; Plasma-polymerization

1. INTRODUCTION

Improving the hydrophobicity of various materials has been a popular topic of research in recent years [1-6]. A high hydrophobicity is useful for a variety of products and industrial uses, such as self-cleaning fabrics and windows, friction reduction in microfluidic devices, glass windshields that quickly evacuate the water for better visibility in adverse weather conditions, solar panels, etc. [1]. Yim et al. [2] deposited hydrophobic coatings with water contact angles in the range of 90-116º on a polymer substrate, using fluorine-based liquid precursors and an atmospheric pressure plasma enhanced vapor deposition process. Recent studies of the self-cleaning ability of presently available hydrophilic and hydrophobic products reveal a higher effectiveness of hydrophilic surfaces for external applications. However, these studies emphasize the importance of the research and development of superhydrophobic surfaces, with water contact angles (WCA) that exceed 150º, because of the excellent self-cleaning ability that they have shown [7]. Generally, the hydrophobicity is improved by two different methods or a combination of both: (1) creation of a rough structure on an intrinsically hydrophobic substrate or (2) modification of a rough surface with low-surface-energy materials [3,8].

For example, Ji et al. [3] used a one-step hydrothermal method to create hierarchical textured morphologies on glass surfaces with water ammonia, and a subsequent modification of the chemical composition with vinyltriethoxysilane. This resulted in superhydrophobic glass surfaces with a water contact angle of 155º. Wu el al. [9] used a sol-gel formula containing hydrophobic polydimethylsiloxane (PDMS) to coat a glass substrate by spraying, in seeking a balance between wear resistance and hydrophobicity. They reported that the wear resistance declined, and the water contact angle increased, as the solution's percentage of PDMS increased. Their optimum PDMS content was 10% by volume. This resulted in a wear resistance that was not significantly compromised, and a high water contact angle (118º) due to the nanoscale surface morphology of the coating obtained.

The development of hydrophobic and wear-resistant surfaces on glass is of particular interest to us because this material is widely used in vehicles and architecture [10]. It is used particularly in photovoltaic cells and parabolic mirrors for photothermal plants in the renewable energy field. The theoretical efficiency limit of solar panels is around 33.7% [7]. Thus, it is very important to approach this limit as closely as possible in order to realize their full capability. This capability is directly reduced as the surface becomes more opaque due to the deteriorating effect of weather agents, cleaning or maintenance work, or by the deposition of dirt and snow. Consequently, the objective of the present work is to study the application of a coating on these surfaces that promotes their hydrophobicity and wear resistance.

For this purpose, the application of different mixtures of liquid precursors has been investigated. (Heptadecafluoro-1,1,2,2-tetrahydrodecyl)trimethoxysilane (FLUSI), is a precursor that is characterized by its low surface energy, due to its fluorocarbon chain. This makes FLUSI a suitable material to increase the hydrophobicity of various substrates. However, these fluorocarbon-based materials can cause problems due to their poor adhesion to metal or inorganic material substrates [11], such as glass. For this reason, it is convenient to combine the fluorinated precursor with an additive that promotes its adhesion and whose behavior governs the mechanical response of the surface [12]. Aminopropyltriethoxysilane (APTES) is one of the materials that are known as aminosilanes. It is the most commonly used reagent to functionalize silica surfaces with amine groups. Aminosilanes have been widely used to promote the adhesion of proteins or different types of molecules to glass or SiO_2 surfaces [13]. Siloxane (SiOSi) is usually formed when aminosilanes are used to apply coatings. Masuko et al. [14] studied the tribological performance of self-assembled monolayers (SAMs) with different numbers of siloxane bonds on smooth silicon substrates. They found that the SAMs with higher numbers of siloxane bonds had stable low friction coefficients and superior durability. Therefore, in our present work, we use APTES to

promote the adhesion of the hydrophobic coating and to improve the wear resistance of the surface.

Among the technologies available for the application of these coatings, the use of a cold or non-equilibrium plasma is especially interesting. This technology allows one to carry out the process at atmospheric pressure and room temperature. In addition, it allows one to control the features of the coatings by the parameters of the plasma-polymerization process, such as gas flow rate, plasma power, etc. This is a versatile technology that is suitable for integration in an in-line process that can apply coatings without altering the substrate's bulk material properties [15,16]. A non-thermal atmospheric jet plasma system will be used, as it is effective for applications, such as depositing coatings that are based on silicon oxide, increasing scratch-resistance and enhancing barrier properties against gases, polyolefins or water [17].

Therefore, we will study various coatings deposited on glass substrate by non-thermal atmospheric jet plasma-polymerization of APTES and FLUSI. In order to find a coating that provides the best balance between hydrophobicity and wear resistance, both precursors will be used individually and mixed in different proportions.

2. EXPERIMENTAL

Glass samples of 100 mm × 50 mm × 3.9 mm were coated by the non-thermal atmospheric jet plasma system, PlasmaSpot® (VITO) [18]. It employs a gun that contains a plasma torch system at atmospheric pressure. This system is equipped with coaxial, cylindrical electrodes and a dielectric barrier of Al_2O_3 between them. The gun moved over the surface of the samples at a fixed speed of 6m/min, keeping a track pitch of 2 mm and a distance of 6 mm from the substrate. All of the samples, except one that was kept uncoated, were subjected first to a surface activation phase by exposure to one pass of plasma without using a precursor. Secondly, each sample was coated by two passes of plasma-polymerization. Nitrogen gas (99.99%) at a flow rate of 80 slm was used as a supply gas for activation and plasma-

polymerization. The generator's power was set at 450 W, and the frequency was set at 68 kHz. The samples were coated using (Heptadecafluoro-1,1,2,2-tetrahydrodecyl)trimethoxysilane (FLUSI, $CF_3(CF_2)_7(CH_2)_2Si(OCH_3)_3$) and aminopropyltriethoxysilane (APTES, $H_2N(CH_2)_3Si(OC_2H_5)_3$) as liquid precursors, both individually and mixed in different proportions as indicated in Table 1.

The specified proportions of the precursors were mixed together in the same container before atomization. An atomizer (model 3076, TSI) was used to nebulize the liquid precursors, producing a fine aerosol. Nitrogen gas at a flow rate of 1.5 slm was used to carry the precursors through the atomizer to the afterglow. This gas flow rate corresponds to a flow rate of approximately 0.06 ml/min for the precursor mixture. The precursors carried by nitrogen gas were admixed perpendicularly to the afterglow through a 0.5 mm opening at the end of the central tube of the gun.

In order to obtain convincing results, some of the analyses were performed on four different sub-samples of 10 mm × 10 mm × 3.9 mm from different locations of each 100 mm × 50 mm × 3.9 mm sample type. The thickness of the coatings was quantified with surface profile measurements using a WYKO NT3300 non-contact surface profiler in phase-shifting interferometry (PSI). Four measurements were taken from each sample in order to obtain an average thickness. Surface images of the samples were taken by a JEOL JSM-840 Scanning Electron Microscope (SEM) at an operating voltage of 10 kV. The wear tracks generated during the tribological tests were observed by a HITACHI S-2400 scanning electron microscope at an operating voltage of 18 kV. A qualitative analysis of the elemental composition of the wear tracks was carried out using an Energy Dispersive X-Ray spectroscope (EDX) Bruker, Quantax 200 with an XFlash 5010/30 detector and microanalysis software ESPRIT 1.9. The surfaces of the samples were coated with gold by sputtering to make them conductive.

Atomic Force Microscopy (AFM) measurements were undertaken in order to study the morphology of the coated and uncoated surfaces. For this purpose, a Multimode AFM from Veeco Instruments operating in tapping mode with a Nanoscope V controller was used. An area of 10 μm × 10 μm was scanned on each sample and the root mean square (RMS) roughness of each sample type was calculated from the images obtained.

Chemical characterization of the coatings was achieved by Fourier Transform Infrared spectroscopy (FTIR) and X-Ray Photoelectron Spectroscopy (XPS) analyses. For the FTIR analysis of the coatings, the same coating process with the same precursors in Table 1 was employed using silicon wafers of 1 cm^2 area as substrates. An uncoated silicon wafer that was subjected to surface activation by one pass of plasma was used as the reference for the comparison of the FTIR spectra. The FTIR spectra were obtained by a BRUKER IFS 66 FTIR spectrometer in transmission mode. The spectrum of each sample was averaged over 64 scans in the range of 400-4000 cm^{-1} with a resolution of 2 cm^{-1}. The FTIR spectra of all samples were normalized according to the peak at 611 cm^{-1}, which is related to the Si-Si of the substrate. To better study the chemical structure of the coatings, the FTIR spectrum of the uncoated substrate was subtracted from those of the coated samples. X-ray photoelectron spectra were obtained using a Physical Electronics PHI 5700 spectrometer with a multi-channel hemispherical analyzer and a MgKα X-ray source (1253.6 eV) operating at 15 kV and 300 W. The spectra were acquired at a constant pass energy of 29.35 eV. The base pressure of the instrument was below 1.33×10^{-7} Pa. An uncoated glass sample that was subjected to surface activation by one pass of plasma was used to better compare the surface chemistry before and after the application of the coatings. Four sub-samples of each sample type were analyzed to obtain each spectrum. A 285 eV binding energy related to the C1s signal for the adventitious carbon was used to reference the peaks of the non-fluorinated samples. A binding energy of 291.4 eV related to CF_2 was used to reference the peaks of the fluorinated samples and compensate the effect of surface charging. The atomic percentage

concentrations of the main elements were calculated from the areas under the photoelectron peaks in the XPS spectra after subtraction of a Shirley-type background. The FTIR spectra after the subtraction and the C1s signal of the XPS spectra of the coated samples were deconvoluted by means of PeakFit 4.12 (SPSS Inc.) software. The spectra were fitted by Gaussian-Lorentzian sum functions allowing variable widths of the peaks. The number and shape of the peaks were constrained.

Lap-shear tests based on the EN 1465:2009 standard were conducted in order to measure the adhesion of the coatings. A machine TRIAX-50 (Controls) with a load cell of 200N was used to measure the fracture load. Four sub-samples of the uncoated glass sample that was subjected to surface activation and of each coated sample were bonded with a 3M-600 tape, in order to perform four tests for each sample type. A cross-head displacement speed of 0.5 mm/min was set for each test, and the lap-shear strength was recorded by a computer. The lap-shear stress of each test was calculated from the maximum strength recorded and the corresponding tested area. The average lap-shear stress value of each coating expressed in MPa of the four lap-shear stress measurements is presented as a measure of its adhesion.

To determine the wettability of the deposited coatings, the static water contact angle (WCA) was measured by the sessile drop method. An OCA15plus system (Dataphysics) and SCA200 software were used for these measurements. Four water drops (3μL/drop) were placed on each sub-sample and the WCA of each sample type, which was expressed as the mean ± standard deviation, was calculated by image analysis. The final result is the average WCA of the four sub-samples.

Tribological tests were conducted to study the wear that the samples experienced from sliding contact in a ball-on-disc setup. A CSM Instruments rotating tribometer was used for this purpose. The counterpart was a 6 mm diameter 100Cr6 steel ball (HRC 60-62). A sliding speed of 2 cm/s, a constant normal load of 1 N, a radius of 2.5 mm and a total sliding distance of 100 m were used in each test. Four sub-samples of each sample type were subjected to

tribological tests. The cross-sectional area of the wear track generated on each sample was measured using a contact profilometer Surtronic 25, Taylor Hobson. Four measurements of each wear track were taken and their mean value was used to calculate the wear rate of the corresponding sample.

3. RESULTS

3.1. Thickness and surface morphology

AFM and SEM analyses of the samples were performed in order to study the relationships between the proportions of APTES and FLUSI used in the plasma-polymerization process and the morphology and roughness of the coating obtained, as well as its thickness (Table 2).

It is known that surface roughness is one of the two main factors that influence hydrophobicity [3,8]. For this reason, the RMS roughness of the uncoated glass and the applied coatings has been studied. As evident in Table 2 and Figures 1(a) and 2(a), the roughness of the uncoated glass substrate is very low (4.9 nm).

Sample A100 has the thickest coating obtained. It also is the smoothest of the coated samples. Furthermore, as the proportion of APTES in the mixtures increases (samples A25/F75, A50/F50 and A75/F25), the coating thickness increases and the roughness decreases (Table 2). In these three cases, the surface morphology varies from an irregular surface with high agglomerates to a more uniform surface with a high density of particles (Figures 1(c, d, e) and 2(c, d, e)).

As can be observed in Table 2, the thickness measured on sample F100 is only 6.3 nm ± 2.7, which is less than its roughness (21.5 nm). Furthermore, the surface of sample F100 is composed of small, dispersed agglomerates that are separated by smooth areas (Fig. 2(b)). These observations denote that a continuous coating has not been achieved by using only FLUSI.

3.2. FTIR analysis

For the transmission FTIR analysis of these coatings, silicon wafers were coated by the same plasma-polymerization process that was used for glass samples. It is assumed that the obtained FTIR spectra are the same as those of the glass samples. To develop a more accurate chemical characterization of the coatings, the spectrum of the activated substrate has been subtracted from the spectra of the coated samples. Thus, the distortion that was introduced by the substrate has been removed. The FTIR spectra of the coatings after the subtraction remain as shown in Fig. 3. The main peaks observed in these spectra are summarized in Table 3. All the spectra before subtraction had an intense band in the range of 530-650 cm^{-1}, with a very strong peak at 611 cm^{-1}. This is due to the Si-Si absorption that is related to the substrate [19]. This common peak has been used to normalize the spectra. The band in 700-990 cm^{-1} (Fig. 3, region A) of the spectrum of the activated substrate shows peaks at ~738 and ~817 cm^{-1}, due to the vibrations of SiC [2] and SiO [20]. The peaks in the range of 835-990 cm^{-1} are related to SiOH stretching [2,21,22]. The only remarkable feature in region A after subtraction is a peak at ~700 cm^{-1}, which is found only in the samples in which APTES was used (Fig. 3, region A). This peak is caused by CH_2 rocking for the ethylene sequence [21]. There is another remarkable band in the range of 1003-1269 cm^{-1} (Fig. 3, region B). The spectrum of the activated substrate has a single sharp peak at ~1105 cm^{-1}, which is typical of silica [23]. This band is broader in the spectra of the coatings. This is due to the overlapping of SiO_2 vibration with those of SiOC, SiOSi and OCH_2CH_3, and the appearance of new peaks at ~1149, ~1200 and ~1236 cm^{-1} that are related to C-F vibration in CF_x (x = 1, 2, 3) [2,12,24,25]. The intensities in the range of 1003-1100 cm^{-1} are related to SiOSi asymmetric stretching mode (ASM) and SiOC groups (Table 3) that form a peak at ~1060 cm^{-1}, which grows as the proportion of APTES increases. For the coatings that are obtained from mixtures of APTES and FLUSI, it is clearly evident that the peaks that are related to CF_x grow as the proportion of FLUSI increases (Fig. 3, region B). In the coating of sample F100, this band has reached lower intensities than in the other coatings.

In the range of 1400-1800 cm^{-1}, all of the spectra show an oscillating band, which is due to the presence of residual water vapor in the spectrometer (Fig. 3, region C). In the range of 1950-2300 cm^{-1} (Fig. 3, region D), Si-H groups that were formed by the silicon of the precursor [12,26] can be identified. In the samples in which APTES was used, the intensity of this band increases with the percentage of APTES. This band appears also in sample F100 with a higher intensity than in samples A25/F75 and A50/F50. This is because the formation of Si-H predominates in sample F100 at the expense of other groups of silicon, such as those identified in region B.

In order to analyze the main constituent groups of the coatings obtained, the subtracted FTIR spectra in the range of 1003-1269 cm^{-1} were deconvoluted (Fig. 4). The peak at ~1035 cm^{-1} is caused by vibrations of SiOSi [2,12]. The peaks at ~1064, ~1115 and ~1162 cm^{-1} are due to SiOC ring-link, open-link and cage-link structures, respectively [18]. The peak at ~1200 cm^{-1} is caused by OCH_2CH_3 [18] in all samples, and also by overlapping with CF_x in the fluorinated coatings [25]. Finally, the peaks at ~1149 and ~1236 cm^{-1} are related to C-F vibrations in CF_x [2,12,24,25].

CF_x groups, especially CF_2 and CF_3 in long chains, are usually related to the reduction of surface energy and, therefore, to the improvement of hydrophobicity by modifying the surface chemistry [2,4,27]. SiOSi is often related to improvements in the tribological properties of coated surfaces [14], such as their wear rate reduction. Because of the importance of these groups, they are studied in more detail.

Fig. 5(a) shows the total absorption areas under the peaks that are related to CF_x in region B (Fig. 4, peaks 4, 6 and 7), although part of the area under Peak 6 corresponds to OCH_2CH_3 from APTES. In sample F100, the presence of CF_x is barely noticeable. In the rest of the fluorinated samples, the areas under the CF_x peaks are much greater and decrease as the proportion of FLUSI employed decreases. In examining the deconvolutions in Fig. 4, one notices that the peak that is related to SiOSi grows as the proportion of APTES used as a

precursor increases. The same evolution is reflected in the area under this peak in Fig. 5(a). These results were normalized proportionally to their corresponding coating thickness, as can be seen in Fig. 5(b). The presence of CF_x groups per unit of thickness keeps the same trend. It is the lowest in sample F100, and it decreases in the rest of the fluorinated samples as the proportion of FLUSI employed decreases. The presence of SiOSi per unit of thickness is practically the same among the samples in which APTES was used, although it still grows slightly as the proportion of APTES used increases. The highest presence of SiOSi per unit of thickness observed in sample F100 is due to the formation of some SiOSi, along with the very low thickness of the coating obtained.

3.3. XPS analysis

An XPS analysis was performed in order to study the relationship existing between the proportions of the precursors used in the plasma-polymerization process and the elemental composition of surfaces obtained. The elemental composition of the samples (in %) of C1s, O1s, Si2p, N1s and F1s appears in Fig. 6.

The 29.4% of carbon measured at the activated glass is probably due to the presence of adventitious carbon on the sample's surface. The carbon percentages of the coated samples are due to both adventitious carbon and carbon provided by the precursors. An examination of Fig. 6 reveals that the chemical composition of the coatings that were applied using APTES (all the coated samples except F100) varies according to the percentage of APTES employed. The percentages of carbon, oxygen, silicon and nitrogen in these samples are directly related to the percentage of APTES. This relationship is inverted for fluorine.

The percentages of all atomic elements in samples A25/F75 and A50/F50 are very similar and include the highest fluorine concentrations of all of the samples (43.6% and 42.2%, respectively).

Since CF_x groups (x = 1, 2, 3) are related to the increase in hydrophobicity [2,4,27], the deconvolution of C1s spectra is undertaken to identify the relative percentage of each of these

groups in Fig. 7. Table 4 summarizes the locations (binding energies) of the peaks considered in the deconvolution of C1s spectra and their corresponding groups. Fig. 8 shows the relative percentages of the different CF_x groups.

The C1s spectra of the fluorinated samples exhibit a peak at ~291.4 eV that is related to CF_2 groups, as well as a certain extension up to ~293.8 eV that corresponds to the CF_3 groups. In the deconvolution of C1s spectra (Fig. 7), one can note that the relative percentage of CF_2 (291.4 eV) depends on the amount of FLUSI used in the mixture. The relative percentage of CF_2 shows the same trend as the F1s percentage in the elemental composition of the surfaces. This is easily appreciated by looking at Fig. 6 and Fig. 8. The peak at ~288 eV was found to have a similar relative percentage in all samples. This is due to the presence of C=O in all samples, regardless of the presence or absence of fluorine on their surfaces. The deposition of different amounts of CF in the fluorinated coatings and the overlapping with the C=O groups at the same binding energy can be the causes of the slight variations that were observed in the relative percentage of this peak (Fig. 8).

3.4. Adhesion

Lap-shear tests were conducted to study the relationship between the proportions of the precursors and the adhesion of the coatings obtained. Fig. 9 shows the average lap-shear stress obtained for each sample type. Samples F100 and A25/F75 had very similar values of lap-shear stress ($6.12 \cdot 10^{-2}$ and $5.79 \cdot 10^{-2}$ MPa), which also are the lowest for all of the coated samples. For the remaining samples, the lap-shear stress increases as the proportion of APTES used increases. Thus, sample A50/F50 has resisted a lap-shear stress of up to $7.19 \cdot 10^{-2}$ MPa, whereas the values obtained for samples A75/F25 and A100 were very similar and the highest ($12.01 \cdot 10^{-2}$ and $13.71 \cdot 10^{-2}$ MPa).

3.5. Wettability

The wettability of the analyzed samples was studied by measuring the static water contact angle (WCA) on their surfaces (Fig. 10). The results of the measurements were very similar

for all sample types in most cases. Thus, the standard deviations shown in Fig.10 are almost negligible, except for sample A100.

As can be seen, the four fluorinated samples acquired a hydrophobic character (WCA > 90º), with maximum WCA values of around 120º.

Uncoated glass exhibits a highly hydrophilic character (WCA < 90º) with a contact angle of 31º ± 0.7. Although sample A100 still has a hydrophilic character, its contact angle (70º ± 6.6) is noticeably greater than that of the uncoated substrate (Fig. 10).

3.6. Wear rate measurements

Tribological tests and profilometry measurements were conducted to study the relationship between the wear rate of the deposited coatings and the proportions of the precursors. In order to determine the wear rate of the samples, a rotating tribometer with the following test parameters was used: a total sliding distance of 100 m with a radius of 2.5 mm, a normal load of 1 N and a sliding speed of 2 cm/s. The counterpart was a 100Cr6 steel ball (HRC 60-62) with a diameter of 6 mm. After the tribological tests had been completed, the cross-sectional area of the wear track that was generated on each sample was measured by a contact profilometer and the corresponding wear rate was calculated.

Fig. 11 shows the wear rate obtained for the uncoated substrate and the samples that were coated with different proportions of APTES and FLUSI. The wear rate of uncoated glass is the highest. It follows from this that any of the tested coatings provide some protection to the surface against wear. Furthermore, the wear rate decreases for the coated samples as the proportion of APTES used increases. This trend is more pronounced among the uncoated glass and the samples that were coated with less than a 50% of APTES (F100, A25/F75).

3.7. Wear mechanisms

SEM images of the wear tracks generated during the tribological tests were taken in order to study the wear mechanisms that operated on the different samples.

In Fig. 12, one can recognize severe wear of the uncoated glass surface. Numerous microcracks, which are characteristics of wear by delamination and fatigue, can be observed inside the wear track (yellow arrows in Fig. 12(b, c)). Propagation of these microcracks leads to material detachment as flake-like debris (white arrow in Fig. 12(c)). This often acts as a third body (white circles in Fig. 12(a, b, c)) and causes abrasive wear. This abrasive wear has caused material loss along the entire wear track (white arrows in Fig. 12(b)). All of these phenomena had been identified by other authors [31].

A tribofilm has formed on the coated samples. For the most part, the tribofilm that formed on sample A25/F75 is smooth (Fig. 13(a), region 1), although it has regions that have suffered wear by delamination and fatigue (Fig. 13(b, c)). Four regions relating to this wear can be identified in Fig. 13(b, c). Cracking of the tribofilm (region 2) occurred first and was followed by detachment of part of its top layer (region 3). Detached wear debris passed through a region of the wear track where the tribofilm had not been formed (region 4) and finally was deposited on both sides of the track (region 5). Some detached wear debris can be seen on the surface of the tribofilm (white circles in Fig. 13(a)).

In the tribofilm of sample A50/F50, one cannot identify the cracks that were observed in the tribofilm of sample A25/F75. Three regions of wear on sample A50/F50 are observed in Fig. 14(b). Region 1 corresponds to the surface of the tribofilm, in which concentric grooves that are generated by the abrasive action of the counterpart can be seen (white arrow in Fig. 14(b)). This wear was not homogeneous, resulting in some zones of more pronounced abrasion of the tribofilm (white arrows in Fig. 14(a)). Wear debris that was generated during the different stages of formation and the subsequent wear of the tribofilm passed through region 2, in which tribofilm had not been formed, and finally was deposited in region 3 on both sides of the wear track.

The tribofilm of sample A100 seems to have suffered less wear than in previous samples. The same grooves that are observed in the tribofilm of sample A50/F50 can be seen in Fig. 15(a,

b). However, the zones of sample A100 that are most worn have a lower extension (white arrows in Fig. 15(a, b)). The same regions, 2 and 3, that were identified on sample A50/F50 are observed.

The tribofilm of sample A25/F75 was analyzed by EDX in order to determine its constituent elements and their origin. EDX maps that appear in Fig. 16 correspond to the image of Fig. 13(c). Among the elements detected by the EDX analysis, the most representative are fluorine (Fig. 16(a)) and iron (Fig. 16(b)). Iron probably is forming iron oxide, since this is the form in which it is normally found in tribofilms [32,33]. Fluorine and iron, which come from the coating and the counterpart respectively, are uniformly distributed in region 1 (Fig. 16(a, b)). In region 2, where tribofilm has detached, the presence of fluorine and absence of iron is observed.

4. DISCUSSION

It has been noted that the higher the percentage of APTES used is, the higher the nitrogen content of the coatings is. Thus, this nitrogen comes mainly from the amines provided by APTES. The lap-shear stress, which generally increases with the percentage of APTES used, shows practically the same trend as the nitrogen content (Fig. 17). That is, both show lower values for coatings that are applied with percentages of APTES up to 50% and reach higher values when APTES is used in a proportion that is equal to 75% or higher (samples A75/F25 and A100). Therefore, an improvement in the adhesion of the coatings that is related to the amines provided by APTES can be seen.

Furthermore, it has been observed that a higher coverage with thicker (Table 2) and more uniform coatings (Fig. 2) is achieved as the percentage of APTES used increases. Considering that the formation rate and transport properties of the reactive species did not vary significantly among different samples due to the fact that the plasma-polymerization parameters were kept constant (flow rate of the mixture of precursors, number of passes, power set on the generator, gap, etc.), the higher presence of amines from APTES that act as a

binder [34] may be one of the reasons that allowed a higher portion of material to adhere during the plasma-polymerization process and facilitated the growth of the coating. As a result, a smooth coating with a greater thickness formed on sample A100. This coating has grown mainly by the deposition of small round particles, which form in the gas phase of the plasma and land on the surface, covering it with a smooth, uniform film (Fig. 1(f)) [35]. The variations that were observed in the surface morphology depend on the proportions of APTES and FLUSI when they are mixed (Fig. 1(c, d, e)). They appear to be due to the difference between the flash points of APTES (96 ºC) and FLUSI (168 ºC). The higher that the percentage of APTES is, the lower the flash point of the mixture is. The flash point is the lowest temperature at which a liquid can vaporize sufficiently to form an ignitable mixture in air. This determines if a gas phase polymerization predominates for lower flash points, or if there is a higher degree of polymerization on the substrate surface for higher flash points [36]. In a work with the same cold plasma source and similar process conditions, Verheyde et al. [37] measured a maximum temperature of 180ºC in the afterglow, whereas the temperature of the substrate did not exceed 90ºC. This range of temperatures can affect the way in which plasma-polymerization takes place, depending on the flash point of the precursor mixture. Thus, the gas phase polymerization mechanism still predominates in sample A75/F25. The addition of a small proportion of FLUSI has led to the formation of larger particles, distributed uniformly over the entire surface (Figures 1(e) and 2(e)). With FLUSI proportions equal to 50% or higher, coatings with more irregular morphologies are formed (Fig. 1(c, d)) mainly by polymerization on the substrate. The origin of these coatings is the precursor's lower fragmentation in the plasma's gas phase, due to the mixture's higher flash point. This has led to the deposition of greater fragments of precursor, such as longer fluorocarbon chains, which undergo polymerization reactions on the surface of the sample [27]. This polymerization has resulted in the formation of agglomerates on samples A25/F75 and A50/F50, which cause their coatings to be rougher. The coating of sample A25/F75 is rougher

because the surface polymerization appears to be more irregular as the percentage of APTES decreases. In the successive passes, an irregular film is deposited over another that has a similar morphology. This results in a rougher and more irregular coating. The poor coverage achieved on sample F100 has resulted in the deposition of small, dispersed agglomerates (Fig. 2(b)) that were formed mainly by polymerization on the surface. The absence of amines in this case is the reason that part of the material has not adhered to the substrate and being evacuated by the exhaust, which has left uncoated areas between the agglomerates. This explains the low thickness measured on this sample and the low intensities shown by its FTIR spectrum after subtraction in the range of 1003-1269 cm^{-1} (Fig. 3, region B). However, it has a noticeable peak in its frequencies that are related to silicon groups and a lower peak at ~1236 cm^{-1}. This may be due to deposition of a small amount of CF_x groups as has been observed by deconvolution (Fig. 5(a)). In turn, this indicates a higher adhesion capability of the part that corresponds to the silicon oxide that is contained in the FLUSI molecule than that of its fluorocarbon chain. Moreover, the poor coverage of sample F100 that is due to the absence of amines from APTES has allowed the XPS analysis to reach the substrate. All of this has caused the percentages of silicon and oxygen in sample F100 to be among the highest for these elements. It also has caused the percentage of fluorine in this sample to be lower than the percentages of fluorine in other samples that were prepared with lower proportions of FLUSI (A25/F75 and A50/F50).

It seems that once APTES is introduced to the mixture of precursors, most of the fluorocarbons provided by FLUSI are able to adhere to the surface. For this reason the amount of fluorine in sample A50/F50 was practically equal to that in sample A25/F75 (Fig. 6), even when the former used a lower amount of FLUSI.

Because the relative percentage of CF_2 shows the same trend as the fluorine percentage of the surfaces, along with the lower percentages of CF and CF_3, one can conclude that almost all of the fluorine that is present on the surfaces of the coatings is part of CF_2 groups. The highest

relative percentages of CF_2 in samples A25/F75 and A50/F50 (Fig. 8) indicate a lower fragmentation of FLUSI in both cases and further preservation of its original structure, with a higher deposition of CF_2 in longer chains of C_xF_y [12,27]. As a consequence, the amounts of CF_x groups in samples A25/F75 and A50/F50 (Fig. 5(a)) are also the highest.

Achieving a hydrophobic character only in the fluorinated samples (Fig. 10) demonstrates that surface chemistry has played a crucial role in the development of hydrophobicity, as it is necessary to deposit functional groups with low surface energy (CF_2 and CF_3) to obtain a hydrophobic surface on the glass substrate. Therefore, the contact angle that was reached mainly by modifying the surface chemistry retained a value of approximately 120º [9]. Moreover, the roughness of these coatings and their surface morphologies have not been sufficiently effective to achieve superhydrophobicity (WCA > 150º).

Considering that the uncoated glass and sample A100 have a similar roughness (Table 2), the higher contact angle of sample A100 may be due to the formation of a uniform coating that contains non-polar CH_3 groups from APTES [5]. WCA values of the coated samples are consistent with the results obtained in the deconvolution of C1s spectra (Fig. 8). The samples with the highest relative percentages of CF_2 (A25/F75 and A50/F50) show the highest values of WCA, since CF_2 has an important influence on the hydrophobic property of the coatings [2,38]. The surface energy of CF_3 is lower than that of CF_2, which makes CF_3 the ideal building block for the development of coatings with higher hydrophobicity [6]. This could explain the higher contact angle of sample A50/F50 (123.2º ± 1.5) in comparison to sample A25/F75 (119.1º ± 1.8), although the latter has a higher relative percentage of CF_2.

The great variation in thickness of the samples prepared with a proportion of APTES that is less than 50% (Table 2) may be the main reason for the decrease in their wear rate. This is not so obvious for the samples that were prepared with higher proportions of APTES (A50/F50, A75/F25 and A100). The thicknesses of the coatings of these three samples are similar (Table 2). The coatings of these samples also are the thickest coatings of all samples. The decrease in

the wear rate in these three cases may be explained by the presence of SiOSi groups that have been identified by FTIR analysis (Fig. 5(a)), which increases as the proportion of APTES used increases. As other authors have found [14], SiOSi groups are related to the formation of hard and wear-resistant coatings.

The spectral shift of the ASM band of SiOSi in the FTIR spectra from 1075 cm^{-1} (related to stoichiometric SiO_2) to ~1035 cm^{-1} indicates a lower stoichiometry constant of the SiO_x in the films ($x < 2$) [22, 39]. This decrease in the stoichiometry constant is related to the carbon content of the samples, which forms several SiOC groups that are identified at higher wavenumbers (Table 3). This is supported by the XPS analysis, in which all samples were found to contain a noticeable percentage of carbon (Fig. 6).

The wear mechanism of the coated samples is governed by a tribofilm that is characteristic of this type of coatings. It is formed in the following stages [32,40]: Severe wear of the surfaces initially takes place, generating wear debris as grains and particles. The part of this debris that is not ejected from the contact zone between the rubbing surfaces is ground, agglomerated and sintered by repeated action of the counterpart. This leads to the formation of a tribofilm, which acts as a protective layer and reduces the initial, severe wear, thus lowering the wear rate [32,41].

Despite its wear, the tribofilm on sample A25/F75 (Fig. 13) achieved a reduction of 41.1% in the wear rate of the uncoated glass (Fig. 11). The tribofilm of sample A100 (Fig. 15) is the most continuous tribofilm. This could explain why its wear rate is the lowest of all of those that were studied [42].

In the EDX maps of Fig. 16(a, b), which showed a region where the tribofilm had been detached (region 2), it can be seen that iron had been removed from that region, although fluorine was still present. It follows that part of the original coating remains even after tribofilm detachment.

5. CONCLUSIONS

In order to find a coating that promotes both the wear resistance and the hydrophobicity of glass, a non-thermal atmospheric jet plasma-polymerization system with mixtures of two precursors at different proportions were used. The precursor FLUSI was used to promote hydrophobicity and the precursor APTES was used to facilitate wear resistance. The greatest drawback of this work was nature of these precursors, since coatings based on FLUSI have a low wear resistance and those based on APTES have a hydrophilic character. For this reason, the key to the present work was determining the optimal mixture of precursors that produces a coating that is satisfactory in both characteristics.

In improving the hydrophobic character of the surface under the present conditions, modifying the surface chemistry by providing CF_x groups has been more effective than modifiying the surface roughness. Thus, all samples in which these groups are present have been hydrophobic with contact angles that exceed 100º, regardless of their low roughness (samples F100 and A75/F25). However, it has not been possible to obtain a superhydrophobic coating (WCA > 150º). The reason is that the roughness of the coatings has been too low to have a sufficient effect on the wettability of the samples. It is estimated that the upper limit of hydrophobicity that can be reached by modifying the surface chemistry (WCA of ∼120º) has been achieved. The amines from APTES promote the adhesion of the fluorinated compounds. It has been noted that wear resistance is affected by large variations in the coating thickness and improves as the thickness increases. Furthermore, the wear resistance of coatings of similar thickness depends on the SiOSi content of the coating. In turn, this is directly related to the proportion of APTES in the mixture of precursors. However, due to the hydrophilic character of its components, high proportions of APTES lead to a decrease in hydrophobicity without significantly increasing wear resistance. The formation of a tribofilm by wear debris from the coating and the counterpart governs the wear mechanism that was identified on the coated samples. The continuity of this tribofilm is determined by the percentage of APTES. The higher that the quality of this tribofilm is, the greater its wear resistance is.

Sample A50/F50 has the only coating in which WCA is greater than 120º. This is mainly because its fluorocarbon content is one of the highest of all samples and its CF_3 content is the highest. Although its wear rate is not the lowest of those achieved by the fluorinated coatings, it is a 50.1% lower than that of the uncoated substrate. As a result of these factors, one can conclude that A50/F50 is the sample that best combines the target properties of hydrophobicity and wear resistance.

In future research, different precursors and mixtures of precursors will be tested in order to improve the results that have been obtained in the target properties. The influence of the plasma-polymerization parameters on coating roughness also will be studied, along with modification of surface chemistry, to achieve a superhydrophobicity of the surface.

Acknowledgments

This work was funded by the Regional Research Plan of the Autonomous Community of La Rioja (Spain) through project FOMENTA 2010/02. One of the authors (ESG) would like to thank the program of predoctoral contracts for the formation of research staff funded by the autonomous community of La Rioja.

References

[1] D.J. Marchand, Z.R. Dilworth, R.J. Stauffer, E. Hsiao, J.-H. Kim, J.-G. Kang, S.H. Kim, Atmospheric rf plasma deposition of superhydrophobic coatings using tetramethylsilane precursor, Surf. Coat. Technol. 234 (2013) 14-20.

[2] J.H. Yim, V. Rodríguez-Santiago, A.A. Williams, T. Gougousi, D.D. Pappas, J.K. Hirvonen, Atmospheric pressure plasma enhanced chemical vapor deposition of hydrophobic coatings using fluorine-based liquid precursors, Surf. Coat. Technol. 234 (2013) 21-32.

[3] H. Ji, G. Chen, J. Yang, J. Hu, H. Song, Y. Zhao, A simple approach to fabricate stable superhydrophobic glass surfaces, Appl. Surf. Sci. 266 (2013) 105-109.

[4] H.-M. Kim, S. Sohn, J.S. Ahn, Transparent and super-hydrophobic properties of PTFE films coated on glass substrate using RF-magnetron sputtering and Cat-CVD methods, Surf. Coat. Technol. 228 (2013) S389-S392.

[5] M.S. Kavale, D.B. Mahadik, V.G. Parale, P.B. Wagh, S.C. Gupta, A.V. Rao, H.C. Barshilia, Optically transparent, superhydrophobic methyltrimethoxysilane based silica coatings without silylating reagent, Appl. Surf. Sci. 258 (2011) 158-162.

[6] R.G. Wankhede, S. Morey, A.S. Khanna, N. Birbilis, Development of water-repellent organic-inorganic hybrid sol-gel coatings on aluminum using short chain perfluoro polymer emulsion, Appl. Surf. Sci. 283 (2013) 1051-1059.

[7] K. Midtdal, B.P. Jelle, Self-cleaning glazing products: A state-of-the-art review and future research pathways, Sol. Energy Mater. Sol. Cells 109 (2013) 126-141.

[8] X. Zhang, Y. Guo, Z. Zhang, P. Zhang, Self-cleaning superhydrophobic surface based on titanium dioxide nanowires combined with polydimethylsiloxane, Appl. Surf. Sci. 284 (2013) 319-323.

[9] Y.L. Wu, Z. Chen, X.T. Zeng, Nanoscale morphology for high hydrophobicity of a hard sol-gel thin film, Appl. Surf. Sci. 254 (2008) 6952-6958.

[10] J. Abenojar, M.A. Martínez, N. Encinas, F. Velasco, Modification of glass surfaces adhesion properties by atmospheric pressure plasma torch, Int. J. Adhes. Adhes. 44 (2013) 1-8.

[11] S. Iwamori, N. Hasegawa, A. Uemura, T. Tanabe, I. Nishiyama, Friction and adhesion properties of fluorocarbon polymer thin films prepared by magnetron sputtering, Vacuum 84 (2010) 592-596.

[12] J. Carpentier, G. Grundmeier, Chemical structure and morphology of thin bilayer and composite organosilicon and fluorocarbon microwave plasma polymer films, Surf. Coat. Technol. 192 (2005) 189-198.

[13] A.R. Yadav, R. Sriram, J.A. Carter, B.L. Miller, Comparative study of solution-phase and vapor-phase deposition of aminosilanes on silicon dioxide surfaces, Mater. Sci. Eng. C 35 (2014) 283-290.

[14] M. Masuko, H. Miyamoto, A. Suzuki, Tribological characteristics of self-assembled monolayer with siloxane bonding to Si surface, Tribol. Int. 40 (2007) 1587-1596.

[15] M. Bashir, J.M. Rees, W.B. Zimmerman, Plasma polymerization in a microcapillary using an atmospheric pressure dielectric barrier discharge, Surf. Coat. Technol. 234 (2013) 82-91.

[16] N. Encinas, B. Díaz-Benito, J. Abenojar, M.A. Martínez, Extreme durability of wettability changes on polyolefin surfaces by atmospheric pressure plasma torch, Surf. Coat. Technol. 205 (2010) 396-402.

[17] M. Laroussi, T. Akan, Arc-free atmospheric pressure cold plasma jets: A review, Plasma Process. Polym. 4 (2007) 777-788.

[18] F. Alba-Elías, E. Sainz-García, A. González-Marcos, J. Ordieres-Meré, Tribological behaviour of plasma-polymerized aminopropyltriethoxysilane films deposited on thermoplastic elastomers substrates, Thin Solid Films 540 (2013) 125-134.

[19] Y. Matsui, S. Adachi, Optical properties of porous silicon layers formed by electroless photovoltaic etching, ECS J. Solid State Sci. Technol. 1 (2012) R80-R85.

[20] V.M. Gun'ko, O. Seledets, J. Skubiszewska-Zięba, V.I. Zarko, R. Leboda, W. Janusz, S. Chibowski, Phosphorus-containing carbon deposits on silica gel Si-100, Microporous and Mesoporous Mater. 87 (2005) 133-145.

[21] F. Alba-Elías, J. Ordieres-Meré, A. González-Marcos, Deposition of thin-films on EPDM substrate with a plasma-polymerized coating, Surf. Coat. Technol. 206 (2011) 234-242.

[22] J. Schäfer, R. Foest, A. Quade, A. Ohl, J. Meichsner, K.D. Weltmann, Carbon-free SiO_x films deposited from octamethylcyclotetrasiloxane (OMCTS) by an atmospheric pressure plasma jet (APPJ), Eur. Phys. J. D 54 (2009) 211-217.

[23] G. Osei-Prempeh, H.-J. Lehmler, A.-F. Miller, B.L. Knutson, S.E. Rankin, Fluorocarbon and hydrocarbon functional group incorporation into nanoporous silica employing fluorinated and hydrocarbon surfactants as templates, Microporous and Mesoporous Mater. 129 (2010) 189-199.

[24] Y. Guo, J. Zhang, J. Xu, J. Yu, Variable morphology of PTFE-like polymer nanocrystals fabricated by oriented plasma polymerization at atmospheric pressure, Appl. Surf. Sci. 254 (2008) 3408-3411.

[25] C.-L. Li, C.-Y. Tu, J.-S. Huang, Y.-L. Liu, K.-R. Lee, J.-Y. Lai, Surface modification and adhesion improvement of expanded poly(tetrafluoroethylene) films by plasma graft polymerization, Surf. Coat. Technol. 201 (2006) 63-72.

[26] D. Rouchon, N. Rochat, F. Gustavo, A. Chabli, O. Renault, P. Besson, Study of ultrathin silicon oxide films by FTIR-ATR and ARXPS after wet chemical cleaning processes, Surf. Interface Anal. 34 (2002) 445-450.

[27] O. Kylián, M. Drábik, O. Polonskyi, J. Čechvala, A. Artemenko, I. Gordeev, A. Choukourov, I. Matolínová, D. Slavínská, H. Biederman, Deposition of nanostructured fluorocarbon plasma polymer films by RF magnetron sputtering of polytetrafluoroethylene, Thin Solid Films 519 (2011) 6426-6431.

[28] A.K. Gnanappa, C. O'Murchu, O. Slattery, F. Peters, B. Aszalós-Kiss, S.A.M. Tofail, Effect of annealing on hydrophobic stability of plasma deposited fluoropolymer coatings, Polym. Degrad. Stab. 93 (2008) 2119-2126.

[29] Y. Pihosh, H. Biederman, D. Slavinska, J. Kousal, A. Choukourov, M. Trchova, A. Mackova, A. Boldyryeva, Composite SiOx/fluorocarbon plasma polymer films prepared by r.f. magnetron sputtering of SiO2 and PTFE, Vacuum 81 (2006) 38-44.

[30] M. Pantoja, N. Encinas, J. Abenojar, M.A. Martínez, Effect of tetraethoxysilane coating on the improvement of plasma treated polypropylene adhesion, Appl. Surf. Sci. 280 (2013) 850-857.

[31] A. Dasari, Z.-Z. Yu, Y.-W. Mai, Fundamental aspects and recent progress on wear/scratch damage in polymer nanocomposites, Mater. Sci. Eng. R 63 (2009) 31-80.

[32] H. Kato, K. Komai, Tribofilm formation and mild wear by tribo-sintering of nanometer-sized oxide particles on rubbing steel surfaces, Wear 262 (2007) 36-41.

[33] W. Chen, Y. Gao, C. Chen, J. Xing, Tribological characteristics of Si3N4-hBN ceramic materials sliding against stainless steel without lubrication, Wear 269 (2010) 241-248.

[34] C. Volcke, R.P. Gandhiraman, V. Gubala, J. Raj, Th. Cummins, G. Fonder, R.I. Nooney, Z. Mekhalif, G. Herzog, S. Daniels, D.W.M. Arrigan, A.A. Cafolla, D.E. Williams, Reactive amine surfaces for biosensor applications, prepared by plasma-enhanced chemical vapour modification of polyolefin materials, Biosens. Bioelectron. 25 (2010) 1875-1880.

[35] A. Michelmore, P. Martinek, V. Sah, R.D. Short, K. Vasilev, Surface morphology in the early stages of plasma polymer film growth from amine-containing monomers, Plasma Process. Polym. 8 (2011) 367-372.

[36] C.E. Nwankire, G. Favaro, Q.-H. Duong, D.P. Dowling, Enhancing the mechanical properties of superhydrophobic atmospheric pressure plasma deposited siloxane coatings, Plasma Process. Polym. 8 (2011) 305-315.

[37] B. Verheyde, D. Havermans, A. Vanhulsel, Characterization and tribological behaviour of siloxane-based plasma coatings on HNBR rubber, Plasma Process. Polym. 8 (2011) 755-762.

[38] G. Borcia, N.M.D. Brown, Hydrophobic coatings on selected polymers in an atmospheric pressure dielectric barrier discharge, J. Phys. D: Appl. Phys. 40 (2007) 1927-1936.

[39] P.G. Pai, S.S. Chao, Y. Takagi, G. Lucovsky, Infrared spectroscopic study of SiO_x films produced by plasma enhanced chemical vapor deposition, J. Vac. Sci. Technol. A 4 (1986) 689-694.

[40] J. Olofsson, S. Jacobson, The influence of grain size and surface treatment on the tribofilm formation on alumina components, Wear 292-293 (2012) 17-24.

[41] M.-S. Suh, Y.-H. Chae, S.-S. Kim, Friction and wear behavior of structural ceramics sliding against zirconia, Wear 264 (2008) 800-806.

[42] P.S. Tantri, E.M. Jayasingh, S.K. Biswas, S.K. Ramasesha, Role of in situ generated tribofilm on the tribological characteristics of monolith and TiB2 reinforced MoSi2 intermetallic, Mater. Sci. Eng. A 336 (2002) 64-71.

TABLES

Table I. Sample identification based on the proportions of APTES and FLUSI.

Sample	Precursors (%)	
	APTES	FLUSI
F100	0	100
A25/F75	25	75
A50/F50	50	50
A75/F25	75	25
A100	100	0
Uncoated glass	-	-

Table II. The coating thickness and RMS roughness of each sample.

Sample	Coating thickness (nm)	RMS roughness (nm)
F100	6.3 ± 2.7	21.5
A25/F75	60.2 ± 9.6	38.9
A50/F50	90.7 ± 22.4	37.8
A75/F25	98.3 ± 7.5	23
A100	105.1 ± 3.5	14.2
Uncoated glass	-	4.9

Table III. Wavenumber and groups related to the FTIR peaks.

Wavenumber (cm^{-1})	Groups	References
611	Si-Si	[19]
~700	CH_2 rocking	[21]
~738	SiC	[2]
~817	SiO	[20]
~1035	SiOSi asymmetric stretching mode (ASM)	[2,12,22]
~1064	SiOC ring-link	[18]
~1115	SiOC open-link	[18]
~1149	CF_x	[2,12,25]
~1162	SiOC cage-link	[18]
~1200	OCH_2CH_3 / CF_x	[2,18,25]
~1236	CF_x	[2,24]

Table IV. Binding energies and functional groups that correspond to the peaks in the deconvolution of C1s spectra.

Peak location (eV)	Functional groups	References
~284.4	C-Si	[2]
~285	C-C, C-H	[2,12,28,29]
~286	C-N	[29,30]
~286.5	C-O	[2,12,28]
~288	C=O, CF	[28,29]
~291.4	CF_2	[2,4,28,29]
~293.8	CF_3	[2,4,28]

LIST OF FIGURE CAPTIONS

Fig. 1. AFM images of the analyzed samples.

Fig. 2. SEM images of the analyzed samples at a magnification of x5000.

Fig. 3. FTIR spectra (500-2500 cm^{-1}) of coated samples after subtracting the substrate spectrum, and FTIR spectrum of the activated substrate. For better clarity, spectra are shown with a vertical spacing.

Fig. 4. FTIR spectra (1003-1269 cm^{-1}) of coated samples after subtracting the substrate spectrum, and their corresponding deconvolution.

Fig. 5. Total area under the peaks related to CF_x and SiOSi in the deconvolution of the subtracted FTIR spectra (1003-1269 cm^{-1}) of the coated samples: (a) obtained from the subtracted FTIR spectra, and (b) normalized proportionally to the coating thickness.

Fig. 6. Elemental composition (%) of sample surfaces.

Fig. 7. Deconvolution of C1s spectra (280-296 eV) of the coated samples.

Fig. 8. Relative percentages of the fluorocarbon groups in the deconvoluted C1s spectra of the fluorinated samples.

Fig. 9. Lap-shear stress sustained by the samples.

Fig. 10. The water contact angle (WCA) of the glass substrate and the coated samples.

Fig. 11. Wear rates of the uncoated glass and the coated samples.

Fig. 12. SEM images of the wear track on uncoated glass at different magnifications: (a) x100, (b) x600 and (c) x2000. Magnifications (b) and (c) are identified by yellow boxes in magnification (a). Dashed arrows indicate the sliding direction of the counterpart over the tested surface.

Fig. 13. SEM images of the wear track on sample A25/F75 at different magnifications: (a) x100, (b) x600 and (c) x2000. Magnifications (b) and (c) are identified by yellow boxes in magnification (a). Dashed arrows indicate the sliding direction of the counterpart over the tested surface.

Fig. 14. SEM images of the wear track on sample A50/F50 at different magnifications: (a) x100 and (b) x1000. Magnification (b) is identified by a yellow box in magnification (a). Dashed arrows indicate the sliding direction of the counterpart over the tested surface.

Fig. 15. SEM images of the wear track on sample A100 at different magnifications: (a) x100 and (b) x600. Magnification (b) is identified by a yellow box in magnification (a). Dashed arrows indicate the sliding direction of the counterpart over the tested surface.

Fig. 16. EDX maps of (a) fluorine and (b) iron from the wear track on sample A25/F75 at a magnification of x2000.

Fig. 17. Lap-shear stress sustained by the coated samples and their atomic percentage of nitrogen.

FIGURES

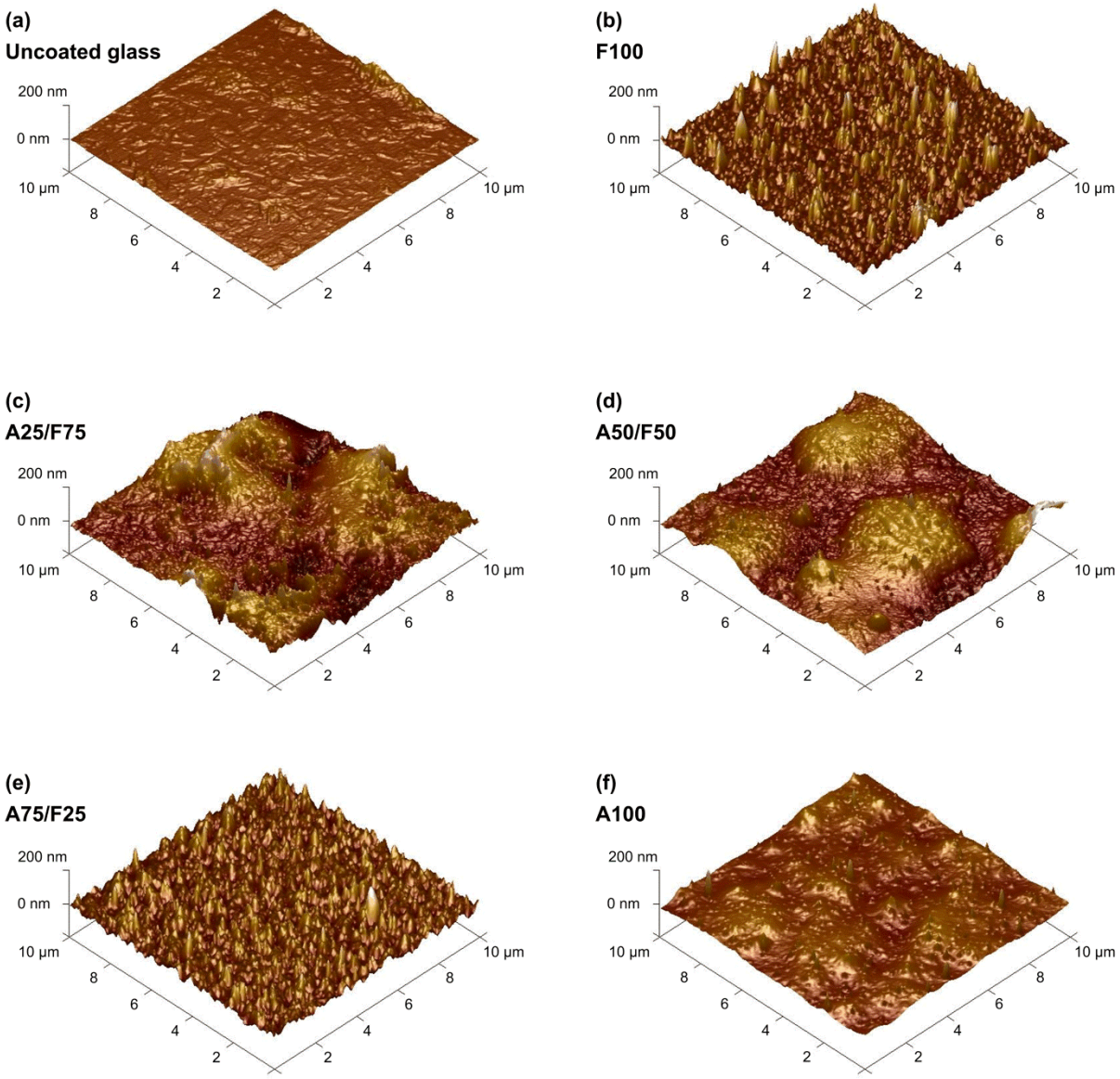

Fig. 1

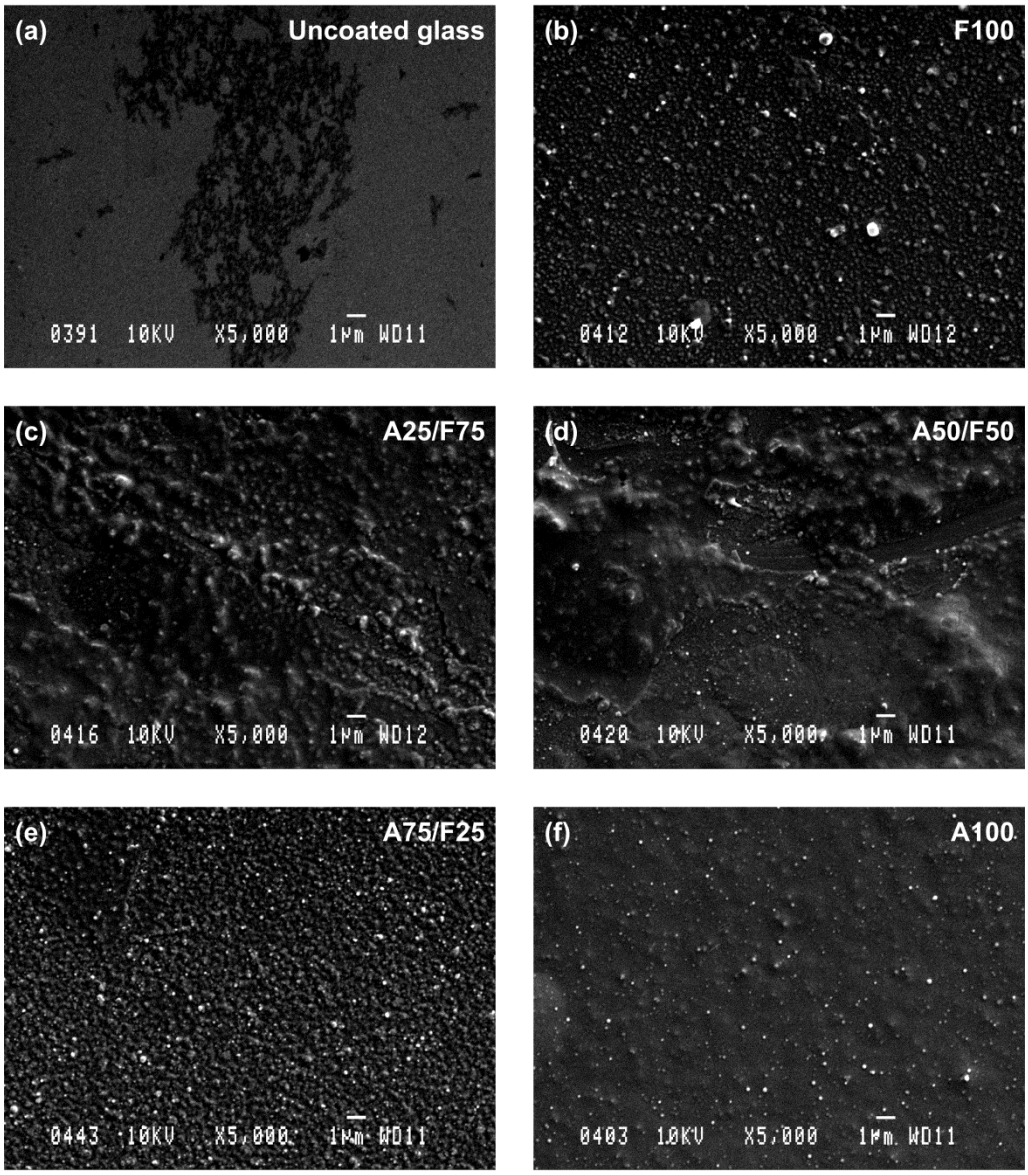
(a)
Uncoated glass
0391 10KV X5,000 1μm WD11
(b)
F100
0412 10KV X5,000 1μm WD12
(c)
A25/F75
0416 10KV X5,000 1μm WD12
(d)
A50/F50
0420 10KV X5,000 1μm WD11
(e)
A75/F25
0443 10KV X5,000 1μm WD11
(f)
A100
0403 10KV X5,000 1μm WD11

Fig. 2

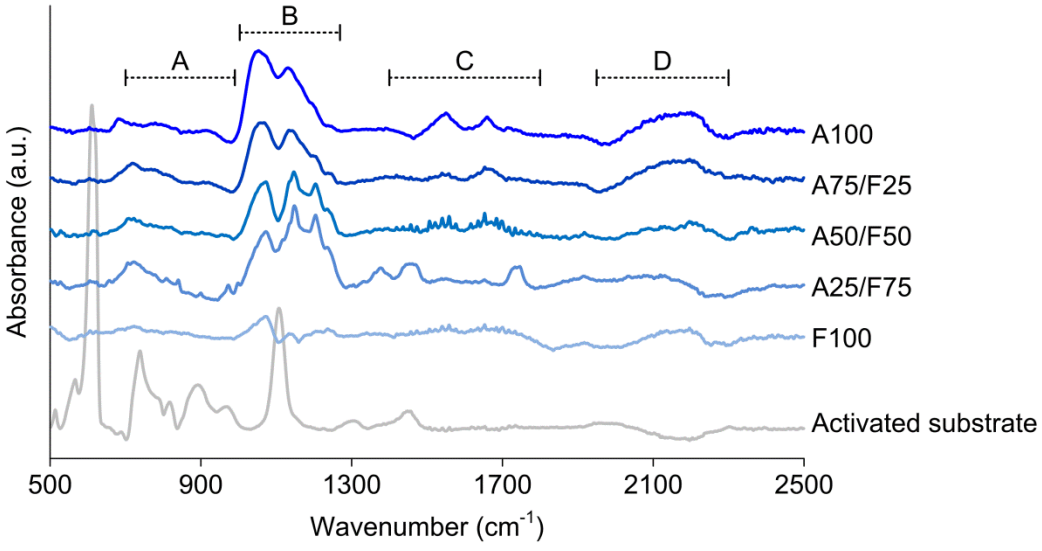
A
B
C
D
A100
A75/F25
A50/F50
A25/F75
F100
Activated substrate
Absorbance (a.u.)
500
900
1300
1700
2100
2500
Wavenumber (cm-1)

Fig. 3

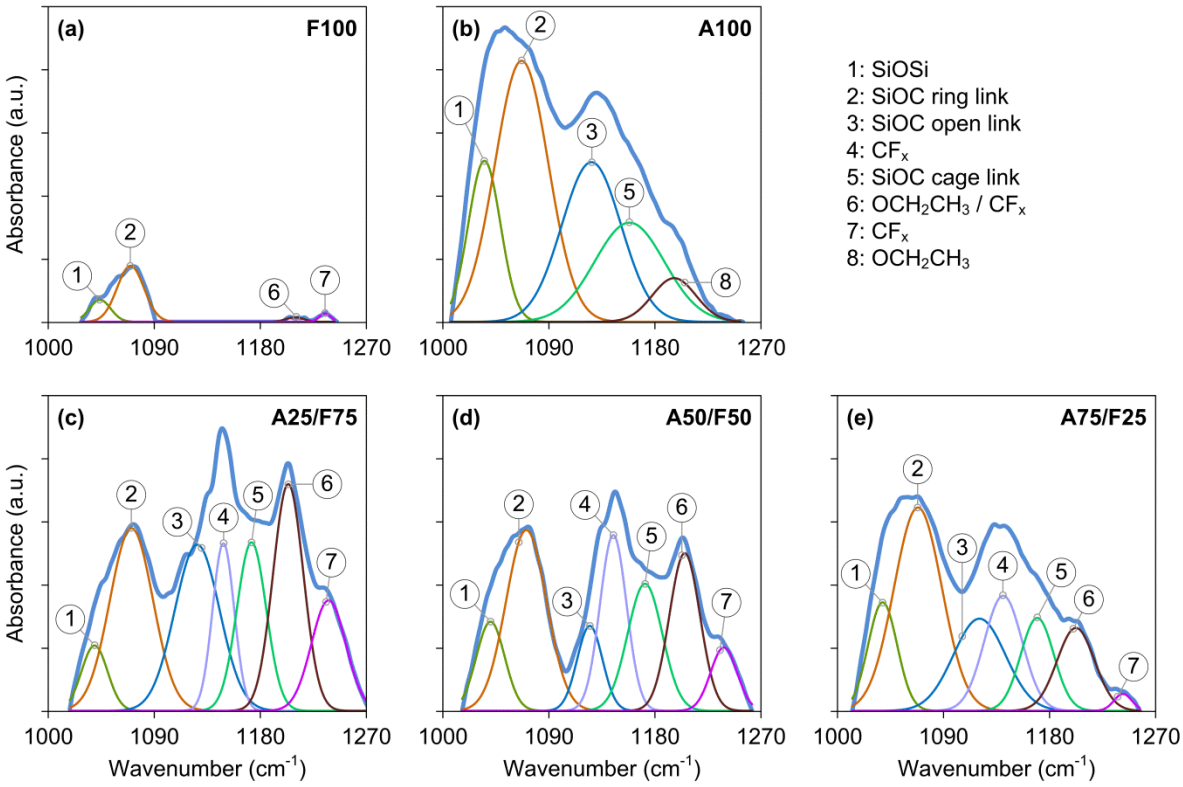
(a) F100
(b) A100
(c) A25/F75
(d) A50/F50
(e) A75/F25
Absorbance (a.u.)
Wavenumber (cm-1)
1000
1090
1180
1270
1: SiOSi
2: SiOC ring link
3: SiOC open link
4: CFx
5: SiOC cage link
6: OCH2CH3 / CFx
7: CFx
8: OCH2CH3

Fig. 4

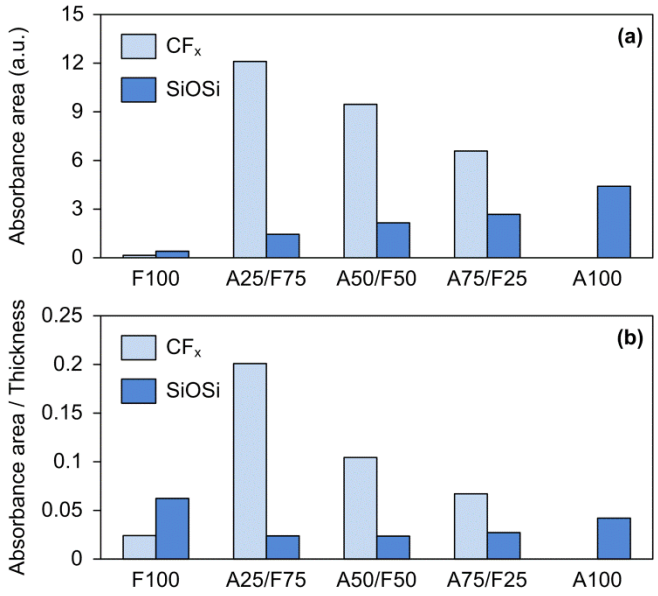
(a)
(b)
CFx
SiOSi
Absorbance area (a.u.)
Absorbance area / Thickness
F100
A25/F75
A50/F50
A75/F25
A100

Fig. 5

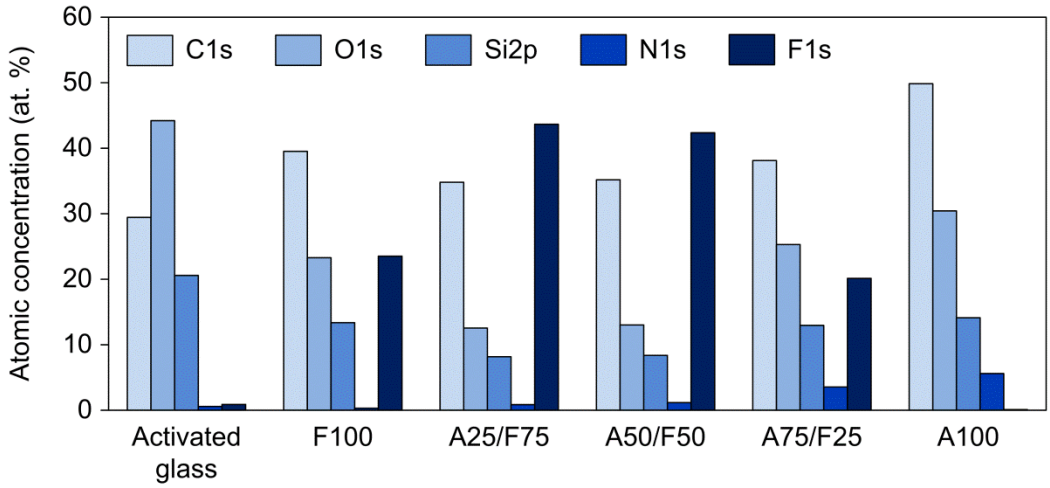

Fig. 6

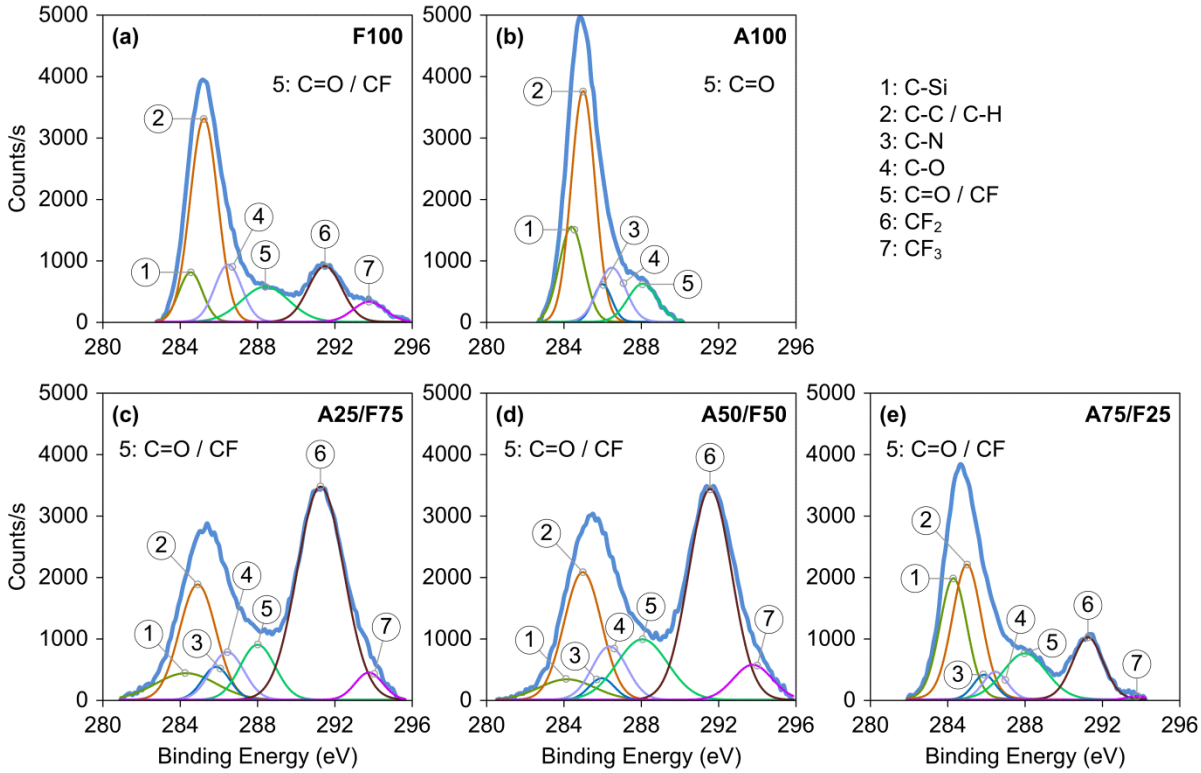

Fig. 7

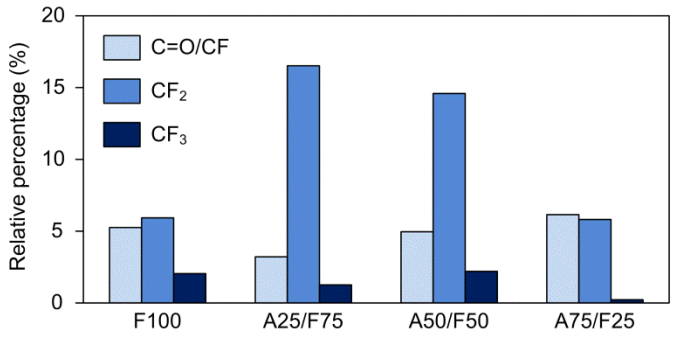

Fig. 8

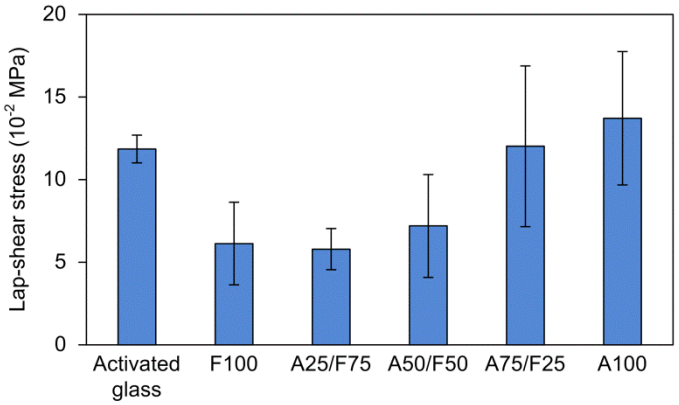

Fig. 9

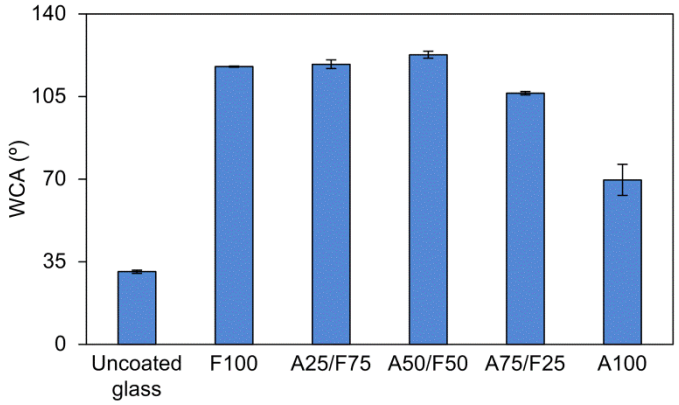

Fig. 10

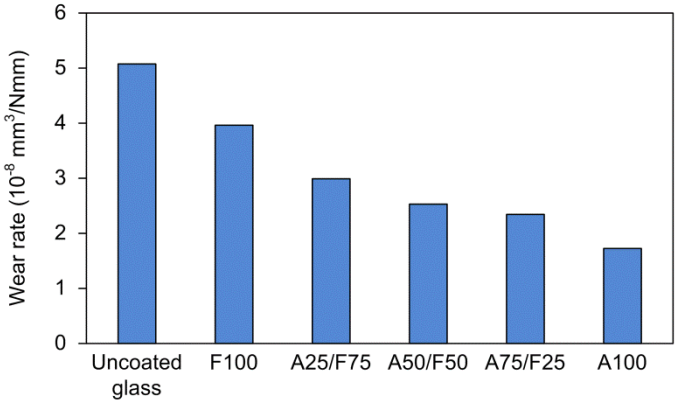

Fig. 11

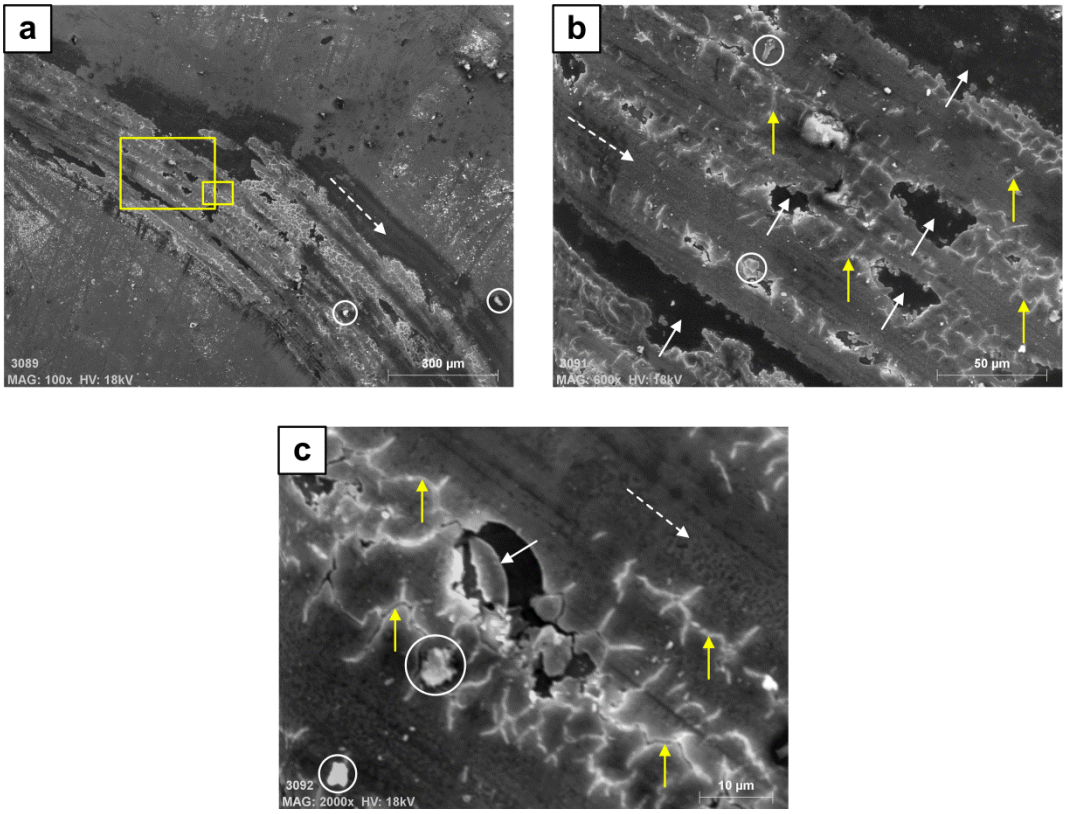
a
3089
MAG: 100x HV: 18kV
300 µm
b
3091
MAG: 600x HV: 18kV
50 µm
c
3092
MAG: 2000x HV: 18kV
10 µm

Fig. 12

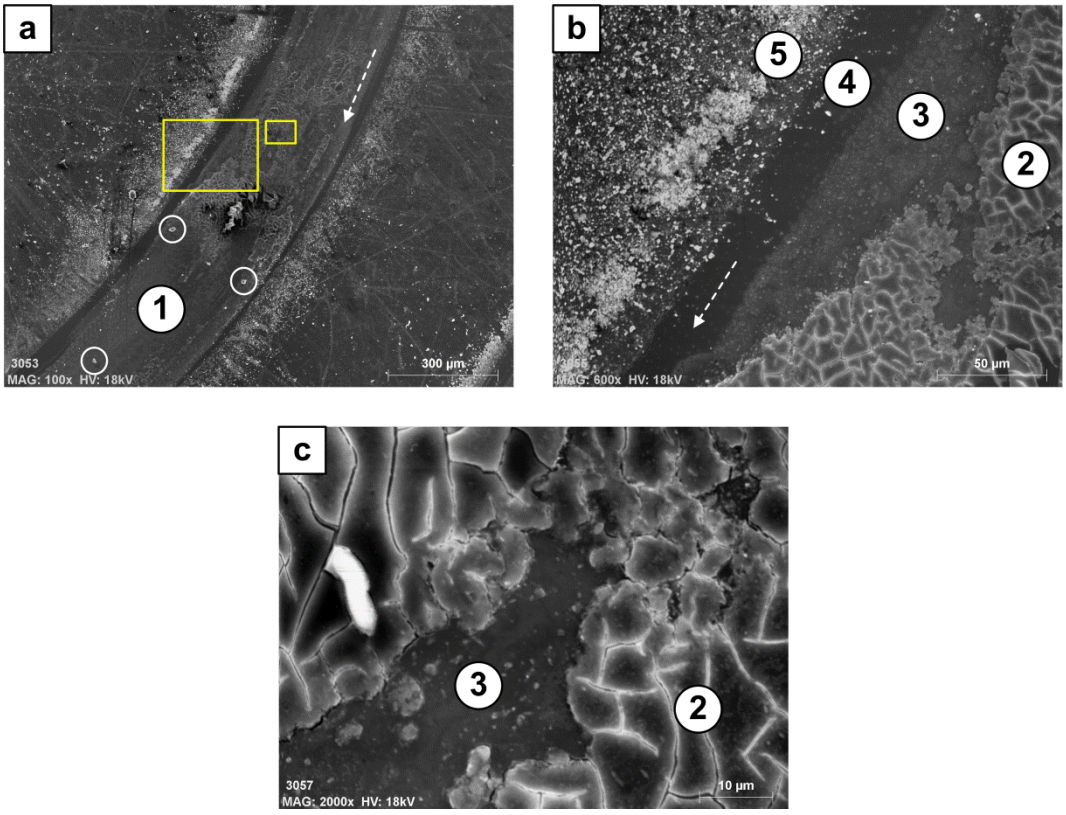
a
1
3053
MAG: 100x HV: 18kV
300 µm
b
5
4
3
2
MAG: 600x HV: 18kV
50 µm
c
3
2
3057
MAG: 2000x HV: 18kV
10 µm

Fig. 13

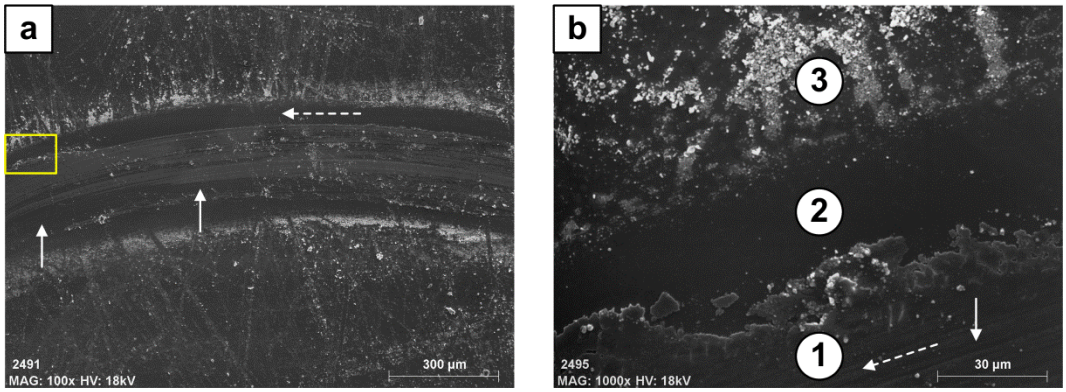

Fig. 14

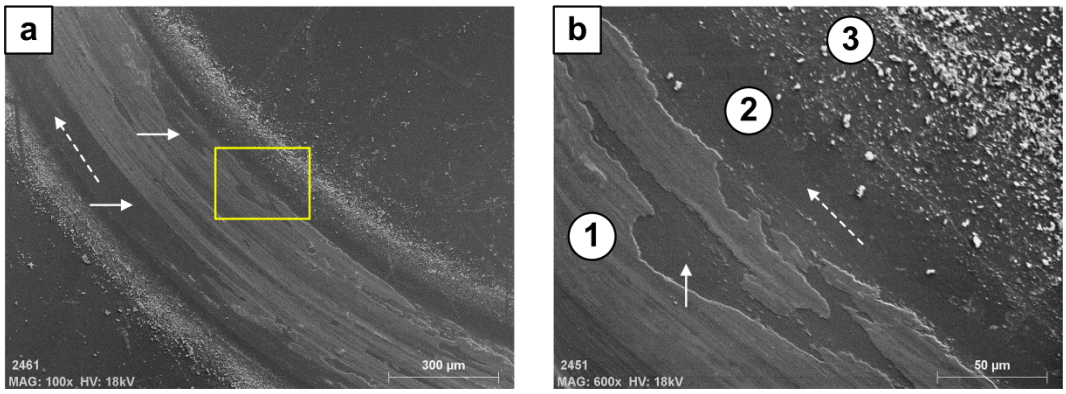

Fig. 15

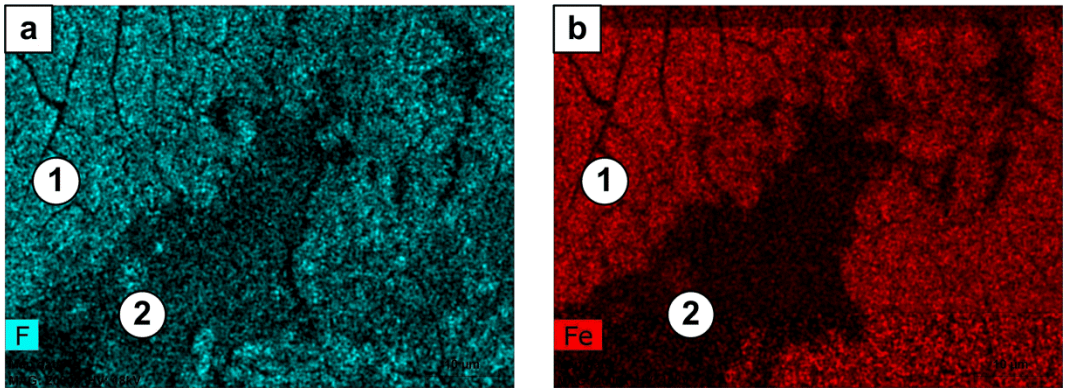

Fig. 16

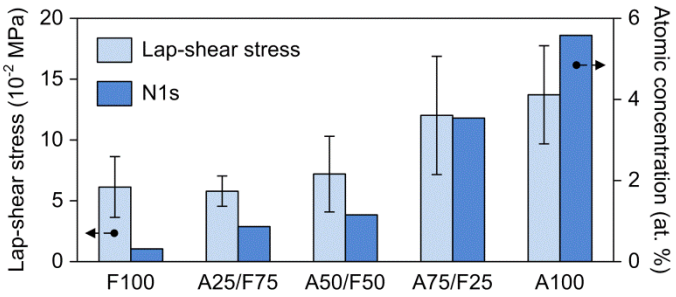

Fig. 17